Heliyon 5 (2019) e01906

Contents lists available at ScienceDirect

Heliyon

journal homepage: www.heliyon.com

S-domain stability analysis of a turning tool with process damping

J.L. Chukwuneke *, C.O. Izuka, S.N. Omenyi

Department of Mechanical Engineering, Nnamdi Azikiwe Univerisity, Awka, Nigeria

ARTICLE INFO

Keywords:
Materials science
Turning tool
Process damping
Stability analysis
S-domain
Speed
Simulation
Modelling

ABSTRACT

This work involved S-domain stability analysis of a turning tool with process damping. Process damping is a phenomenon of dry friction between the tool flank face and workpiece which induces high stability and smoothness at low turning speed. A pair of valid equations for stability analysis of turning with process damping was derived in this work using Laplace transformation method. This work for the first time introduced non-linear feed term in the existing process damping model leading to process damping force of form $F_{pd}(v\tau)^{\alpha}$ where F_{pd} processed damping force model in related literature. It is seen that in light of experiments of the related literature, the new proposal can only be valid for low values of α in the neighbourhood of 0.01. MATLAB delay differential equation solver called dde23 was used to simulate the vibration response of turning processes at selected points on the stability diagram of turning with and without process damping. This helped in confirming that stable points in the stability diagram of turning with process damping became unstable points in the stability diagram of turning without process damping. The stability was much higher at low speed of 200rpm than at speed of 4000rpm. Process damping coefficient C_{pd} of the experiment was estimated at C_{pd} of 61,000 N/m by comparing experimental depths of cut with theoretical depths of cut of known process damping coefficient.

1. Introduction

Production of mechanical parts for engineering and technological applications is accomplished by various machining operations. The turning process is one of the basic material removal processes holds a dominant position in manufacturing practices due to its wide range of application in the industry [1, 2, 3].

In turning operation, which is widely used in the manufacturing of automotive, agricultural and aerospace parts, a cutting tool removes material when it is fed into a rotating workpiece. Modelling and stability analysis of machining dynamics is known to be very useful in the optimal choice of cutting conditions for a given machine tool-spindle-tool holder-cutting tool and workpiece system [4, 5, 6, 7]. The normal practice has been to base the selection of cutting conditions on the experience of the machinist, handbook guidelines or specifications of catalogues of cutting tools and machine tools. Such unaided method of selection is laborious and unreliable because of parameter changes with variation of machine tool-spindle-tool holder-cutting tool and workpiece system. Poor selection of cutting conditions could lead to the following problems; Chatter vibrations [8, 9, 10, 11, 12, 13], widely varying cutting forces that lead to tool breakage and structural failure, violation of machine tool capacity or limit leading to system failure [14] and excessive tool wear [15] during machining. Some of the advantages of analytical modelling of dynamics and stability of turning process include avoidance of poor surface finish, workpiece damage and violation of tolerance limits, reduced time and cost, reduced wastage and improvement of machine tool spindle working life [16]. For a given machine tool-spindle-tool holder-cutting tool and workpiece system, the main objective of dynamic analysis is to select chatter-free cutting conditions with lower cutting forces while respecting the power and torque limits of machine tools and other practical constraints of turning system.

Among other operations on the lathe, cutting tools are used for both facing and turning operations. It is known in the workshop that machining productivity is marred by violent chatter vibrations [1, 2]. As already mentioned one option for handling the problem of chatter in workshops is by stability analysis that leads to differentiation of cutting parameter space into stable and unstable domains.

The modal parameters like damping ratio and natural frequency are

* Corresponding author.
E-mail address: jl.chukwuneke@unizik.edu.ng (J.L. Chukwuneke).

https://doi.org/10.1016/j.heliyon.2019.e01906
Received 19 January 2019; Received in revised form 24 March 2019; Accepted 3 June 2019

needed for stability analysis of turning tools. Modal parameters are normally determined via experimental modal analysis. During machining, energy is supplied to the tool from the machining process thus the arising excitations are called self-excitations. Self-excitations are successfully weakened by the structural damping of the tool when the rate of energy supply is less than the rate of energy dissipation. When the rate of energy supply is overbearing on the rate of energy dissipation instability grows. Process damping is a very helpful phenomenon at low speeds because it considerably enhances damping thus improving stability [17, 18].

Ozoegwu [19] presented a detailed stability analysis of turning process with no process damping using the method of D-subdivision. This work aims at arriving at the same set of stability equations using Laplace transformation method. Other works dealing with process damping in surveyed literature presented their stability equations differently. Most of the works have analyzed the turning process with the frequency response approach. The most recent of the reviewed works is that of Tyler and Schmitz [10, 20] which derived stability equations of the turning process (with or without process damping) with the frequency response approach. Thus, their stability equations have a different look from those of Ozoegwu [19]. Another unique thing with this work is that the process damping model of Tyler and Schmitz [20] will be incorporated in the turning stability equations, also to be derived in this work using Laplace transformation and analysis. The results will be validated with the results of Tyler and Schmitz [20]. Exploration for a possible avenue for modification of process damping model of Tyler and Schmitz [20] will be made.

2. Methodology

2.1. Equipment and tools

The lathe machine used has a spindle speed range of $100-5000$ *rpm*. The cutting tool used is High-Speed Steel (HSS) and the workpiece is AISI 1018. The combination was made so to allow deep depths of cut owing to the fact that machinability is a factor of the correct combination of hardness and ductility. Three spindle speeds (200 *rpm*, 1000 *rpm* and 4000 *rpm*) were chosen for experimental analysis, at each speed, depth of cut was changed gradually from zero in steps of 0.5 *mm* until initially quiet machining process becomes noisy (above 85 *decibels*, dB), measured with the aid of a Sound Level Meter. The violent sound energy is an indicator of chatter. The experimental set-up is shown in Fig. 1.

2.2. Dynamical stability of turning process with process damping

The process damping effect manifests an increase of the chatter-free chip widths (depth of cut) at low speeds. This augmented stability at low spindle speeds is particularly imperative for hard-to-machine materials that cannot take benefit of the higher speed stability zones (lobbing effect) owing to prohibitive tool wear at high cutting speeds.

I. Modelling of Process Damping in Turning Process

Various process damping models exist in literature. The model that will form the backbone of this work is that proposed by Tyler and Schmitz [10, 20]. This model is chosen because an avenue for its modification is identified and will be highlighted subsequently. Tyler and Schmitz [10, 20] considered a tool moving on a sine wave (vibration mark) while shearing away the chip. The process damping force F_{pd}, in the y-direction can be expressed as linearly proportional to vibration velocity $\dot{x}(t)$ and depth of cut w and inversely proportional to the cutting speed v_c [21, 22]:

$$F_{pd} = -C_{pd}\frac{w}{v_c}\dot{x}(t) \tag{1}$$

The constant of proportionality C_{pd} is called the process damping coefficient. It must be noted that steeper sinusoidal surface will increase the amplitude of the F_{pd} and thus make the damping effect larger. This will occur when vibration wavelengths get shorter or when the amplitude of vibration increases. The cutting speed v_c being the wave velocity is related to the wavelength λ and frequency f_w by

$$v_c = \lambda f_w \tag{2}$$

This shows that higher vibrating frequenciesf_w, give shorter wavelengths and subsequently increased process damping. The cutting speed v_c is related to the spindle speed by Ω;

$$v_c = \frac{\pi}{60}\Omega D \tag{3}$$

Where D is the diameter of cutting. The wavelength can be expressed as

$$\lambda = \frac{\pi}{60 f_w}\Omega D \tag{4}$$

Eq. (4) clearly shows that wavelengths are shorter and process damping higher when spindle speeds are smaller. In light of equation (3), equation (1) becomes

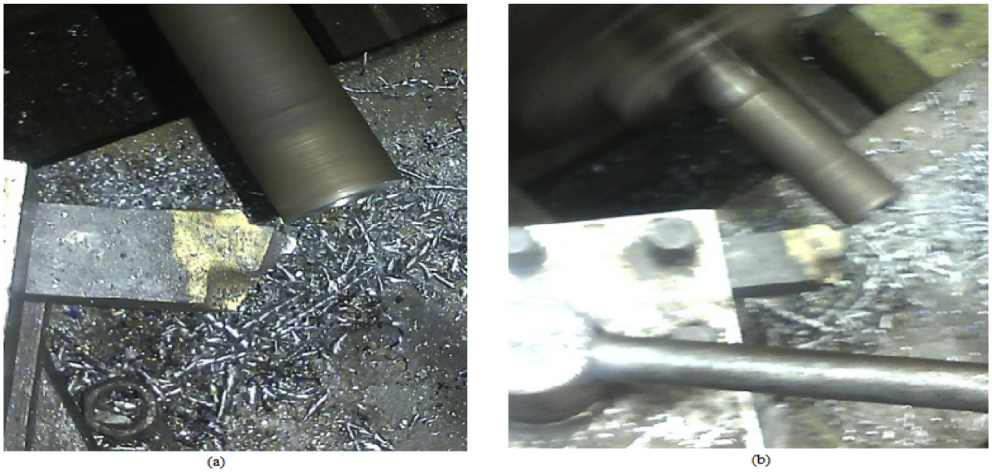

Fig. 1. Experimental set-up a) Non-cutting mode, b) Cutting mode.

$$F_{pd} = -\frac{60}{\pi} C_{pd} \frac{w}{\Omega D} \dot{x}(t) \tag{5}$$

The dynamical model of the turning process by [23, 24, 25] is;

$$m\ddot{x}(t) + c\dot{x}(t) + kx(t) = F_x(t) \tag{6}$$

Incorporating Eq. (5) in Eq. (6) gives the differential equation of motion as

$$m\ddot{x}(t) + \left[c + \frac{60}{\pi} C_{pd} \frac{w}{\Omega D}\right] \dot{x}(t) + kx(t) = F_x(t) \tag{7}$$

With the substitution $F_x(t) = Cw[x(t) - x(t-\tau)]$, Eq. (7) is written in modal form;

$$\ddot{x} + \left[2\xi\omega_n + \frac{60}{\pi} C_{pd} \frac{w}{\Omega D m}\right] \dot{x} + \omega_n^2 x = \frac{Cw}{k} \omega_n^2 [x(t) - x(t-\tau)] \tag{8}$$

It is seen from Eq. (8) that equivalent specific viscous damping approaches $2\xi\omega_n$ when Ω rises meaning that process damping diminishes with the rise in speed. It must be noted that the analysis of Eq. (8) is very similar to the analysis of Eq. (7) presented in the preceding section. The only difference between the two analyses is that is replaced with $2\xi\omega_n + \frac{60}{\pi} C_{pd} \frac{w}{\Omega D m}$. The pair of equations for critical parameter combinations becomes

$$w_c = \frac{-m}{2C} \frac{\left(\omega_n^2 - \omega^2\right)^2 + \left(2\xi\omega_n + \frac{60}{\pi} C_{pd} \frac{w_c}{\Omega_c D m}\right)^2 \omega^2}{\left(\omega_n^2 - \omega^2\right)} \tag{9}$$

$$\Omega_c = 30\omega \left\{ l\pi - \tan^{-1}\left(\frac{\omega_n^2 - \omega^2}{-\left[2\xi\omega_n + \frac{60}{\pi} C_{pd} \frac{w_c}{\Omega_c D m}\right]\omega} \right) \right\}^{-1}, \quad l = 1,\ 2,\ 3,\ \ldots\ldots\ldots \tag{10}$$

Eqs. (9) and (10) are similar to equations in Ozoegwu [19] but with further complication of containing w_c and Ω_c on the right-hand side. Iterative computation is needed in order to arrive at stability lobes of turning with process damping using Eqs. (9) and (10). The iterative computation is represented in four equations as follows;

$$w_{c,1} = \frac{-m}{2C} \frac{\left(\omega_n^2 - \omega^2\right)^2 + 4\xi^2\omega_n^2\omega^2}{\left(\omega_n^2 - \omega^2\right)} \tag{11}$$

$$\Omega_{c,1} = 30\omega \left\{ l\pi - \tan^{-1}\left(\frac{\omega_n^2 - \omega^2}{-2\xi\omega_n\omega} \right) \right\}^{-1} \quad l = 1,\ 2,\ 3,\ \ldots\ldots\ldots \tag{12}$$

$$w_{c,i+1} = \frac{-m}{2C} \frac{\left(\omega_n^2 - \omega^2\right)^2 + \left(2\xi\omega_n + \frac{60}{\pi} C_{pd} \frac{w_{c,i}}{\Omega_{c,i} D m}\right)^2 \omega^2}{\left(\omega_n^2 - \omega^2\right)} \tag{13}$$

$$\Omega_{c,i+1} = 30\omega \left\{ l\pi - \tan^{-1}\left(\frac{\omega_n^2 - \omega^2}{-\left[2\xi\omega_n + \frac{60}{\pi} C_{pd} \frac{w_{c,i}}{\Omega_{c,i} D m}\right]\omega} \right) \right\}^{-1}, \quad l = 1,\ 2,\ 3,\ \ldots\ldots\ldots \tag{14}$$

Where $i = 1,\ 2,\ 3,\ \ldots\ldots\ldots$ The system is considered to have converged at the *nth* iteration if

$$w_{c,n} = \frac{-m}{2C} \frac{\left(\omega_n^2 - \omega^2\right)^2 + \left(2\xi\omega_n + \frac{60}{\pi} C_{pd} \frac{w_{c,n-1}}{\Omega_{c,n-1} D m}\right)^2 \omega^2}{\left(\omega_n^2 - \omega^2\right)} \approx w_{c,n-1} \tag{15}$$

$$\Omega_{c,n} = 30\omega \left\{ l\pi - \tan^{-1}\left(\frac{\omega_n^2 - \omega^2}{-\left[2\xi\omega_n + \frac{60}{\pi} C_{pd} \frac{w_{c,n-1}}{\Omega_{c,n-1} D m}\right]\omega} \right) \right\}^{-1} \approx \Omega_{c,n-1}, \tag{16}$$

A typical accuracy could be stated as a per cent difference between subsequent minimum values. The critical depth of cut w_c will subsequently be plotted as a function of critical spindle speed Ω_c to generate the stability lobes of systems with process damping.

II. Proposal for Slight Modification of the Existing Model

The tool is being fed into the workpiece normal to the surface wave. It is rational to suspect that the magnitude of feed will have an effect on the magnitude of process damping force. Reason being that higher feed will exert higher thrust force on the tool flank. This reasoning is reminiscent of the fact that the cutting force of orthogonal cutting is given by Eq. (17). It is noted that non-chatter turning process means that the time-dependent feed;

$$f_x(t) = x(t) - x(t-\tau) \tag{17}$$

Therefore, the prescribed feed:

$$f_x = v\tau \tag{18}$$

The non-linear force model used by [19, 24] gives Eq. (17) the form

$$f_x = (v\tau)^\gamma \tag{19}$$

Where γ is a less-than-unity positive exponent. By this line of reasoning it is proposed that the process damping force is directly proportional to some other positive power of feed of the non-chatter turning, thus

$$F_{pd} = -\frac{60}{\pi} C_{pd} \frac{w}{\Omega D} (v\tau)^\alpha \dot{x}(t) \tag{20}$$

Eq. (20) is re-written with the substitution $\tau = 60/\Omega$ to become

$$F_{pd} = -\frac{60^{1+\alpha}}{\pi} C_{pd} \frac{w}{\Omega^{1+\alpha} D} v^\alpha \dot{x}(t) \tag{21}$$

Incorporating Eq. (21) in Eq. (6) gives the differential equation of motion as

$$m\ddot{x}(t) + \left[c + \frac{60^{1+\alpha}}{\pi} C_{pd} \frac{w}{\Omega^{1+\alpha} D} v^\alpha\right] \dot{x}(t) + kx(t) = F_x(t) \tag{22}$$

Replacing the cutting force with $F_x(t) = Cw[x(t) - x(t-\tau)]$, Eq. (22) is written in modal form as

$$\ddot{x} + \left[2\xi\omega_n + \frac{60^{1+\alpha}}{\pi} C_{pd} \frac{w}{\Omega^{1+\alpha} D m} v^\alpha\right] \dot{x} + \omega_n^2 x = \frac{Cw}{k} \omega_n^2 [x(t) - x(t-\tau)] \tag{23}$$

The pair of equations for critical parameter combinations under the current proposal becomes

$$w_c = \frac{-m}{2C} \frac{\left(\omega_n^2 - \omega^2\right)^2 + \left(2\xi\omega_n + \frac{60^{1+\alpha}}{\pi} C_{pd} \frac{w_c}{\Omega_c^{1+\alpha} D m} v^\alpha\right)^2 \omega^2}{\left(\omega_n^2 - \omega^2\right)} \tag{24}$$

$$\Omega_c = 30\omega \left\{ l\pi - \tan^{-1}\left(\frac{\omega_n^2 - \omega^2}{-\left[2\xi\omega_n + \frac{60^{1+\alpha}}{\pi} C_{pd} \frac{w_c}{\Omega_c^{1+\alpha} D m} v^\alpha\right]\omega} \right) \right\}^{-1}, \tag{25}$$

$l = 1,\ 2,\ 3,\ \ldots\ldots\ldots$

The iterative computation is represented in four equations as follows

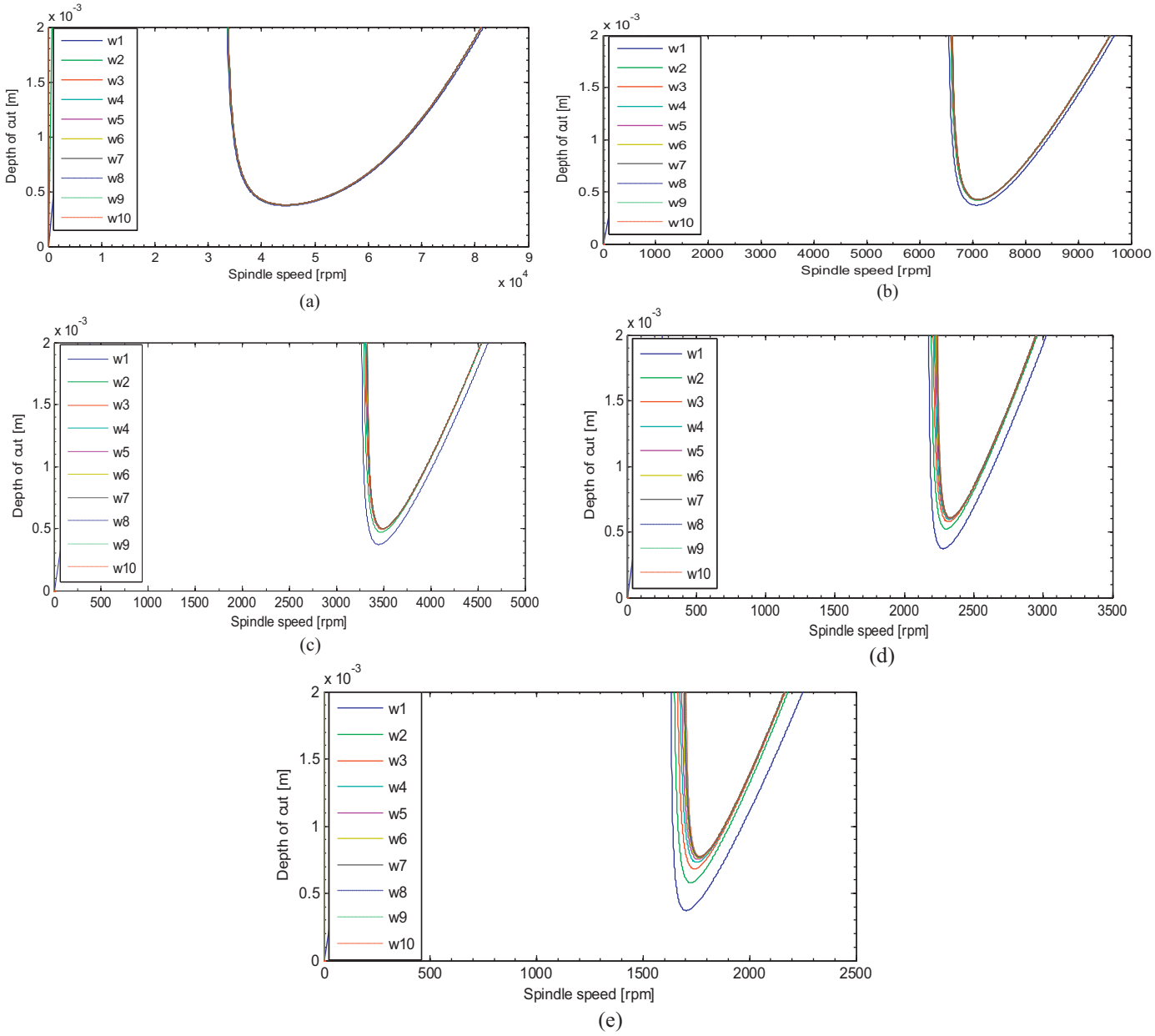

Fig. 2. Ten iterations of turning process as modelled using the Tyler and Schmitz [20] process damping model leading to the generation of a) the first lobe, b) the fifth lobe, c) the tenth lobe, d) the fifteenth lobe, e) the twentieth lobe.

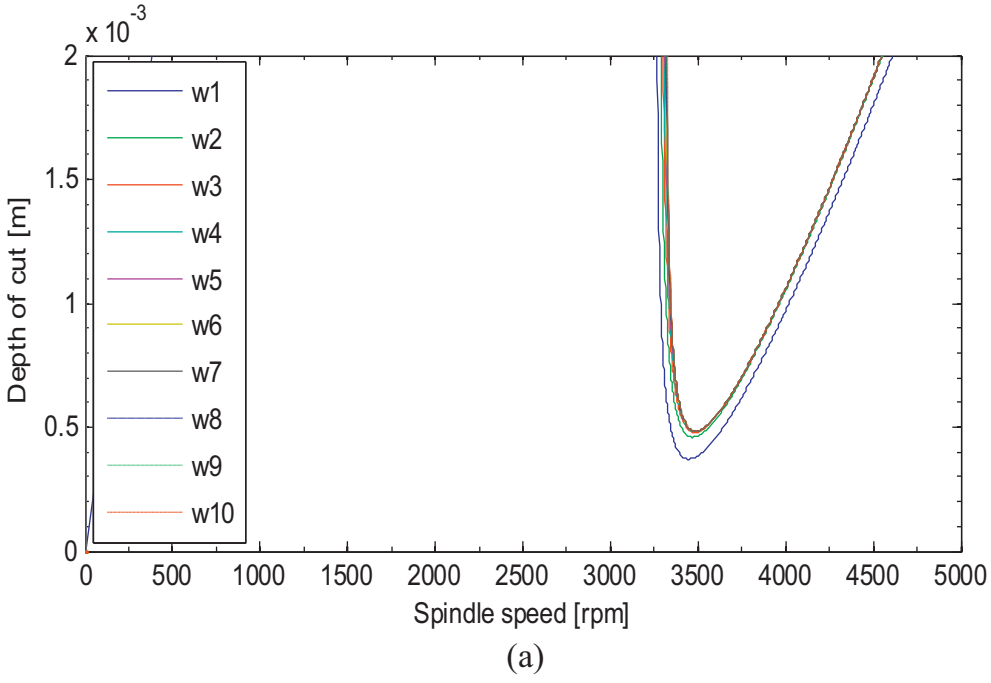

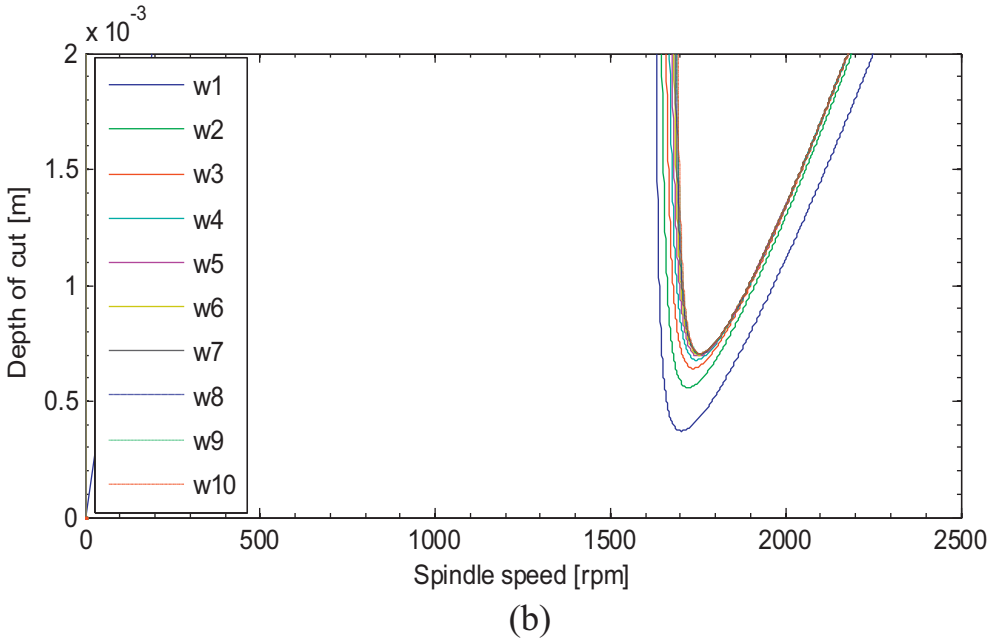

Fig. 3. Ten iterations of the proposed process damping model a) $\alpha = 0.01$ leading to the generation of the tenth lobe, for b) $\alpha = 0.01$ leading to the generation of the twentieth lobe.

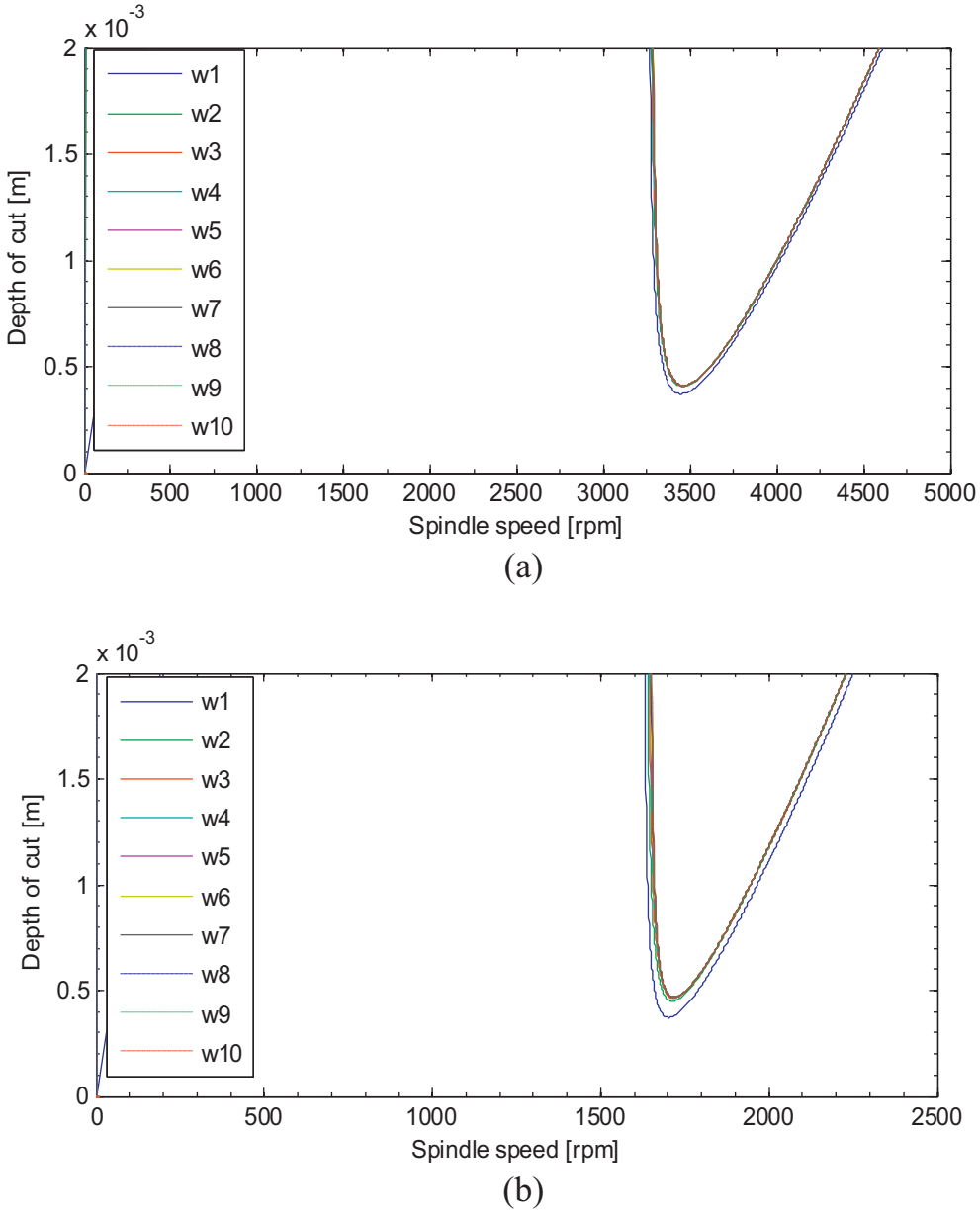

Fig. 4. Ten iterations of the proposed process damping model a) $\alpha = 0.1$ leading to the generation of the tenth lobe, b) $\alpha = 0.1$ leading to the generation of the twentieth lobe.

$$w_{c,1} = \frac{-m}{2C}\frac{\left(\omega_n^2 - \omega^2\right)^2 + 4\xi^2\omega_n^2\omega^2}{\left(\omega_n^2 - \omega^2\right)} \tag{26}$$

$$\Omega_{c,1} = 30\omega\left\{l\pi - \tan^{-1}\left(\frac{\omega_n^2 - \omega^2}{-2\xi\omega_n\omega}\right)\right\}^{-1} \quad l = 1,\ 2,\ 3,\ \ldots\ldots\ldots \tag{27}$$

$$w_c = \frac{-m}{2C}\frac{\left(\omega_n^2 - \omega^2\right)^2 + \left(2\xi\omega_n + \frac{60^{1+\alpha}}{\pi}C_{pd}\frac{w_{c,i}}{\Omega_{c,i}{}^{1+\alpha}Dm}v^{\alpha}\right)^2\omega^2}{\left(\omega_n^2 - \omega^2\right)} \tag{28}$$

$$\Omega_c = 30\omega\left\{l\pi - \tan^{-1}\left(\frac{\omega_n^2 - \omega^2}{-\left[2\xi\omega_n + \frac{60^{1+\alpha}}{\pi}C_{pd}\frac{w_{c,i}}{\Omega_{c,i}{}^{1+\alpha}Dm}v^{\alpha}\right]\omega}\right)\right\}^{-1}, \quad l = 1,\ 2,\ 3,\ \ldots\ldots\ldots \tag{29}$$

Where $i = 1,\ 2,\ 3,\ \ldots\ldots\ldots$ The system is considered to have converged at the *nth* iteration if

$$w_c = \frac{-m}{2C}\frac{\left(\omega_n^2 - \omega^2\right)^2 + \left(2\xi\omega_n + \frac{60^{1+\alpha}}{\pi}C_{pd}\frac{w_{c,n-1}}{\Omega_{c,n-1}{}^{1+\alpha}Dm}v^{\alpha}\right)^2\omega^2}{\left(\omega_n^2 - \omega^2\right)} \approx w_{c,n-1} \tag{30}$$

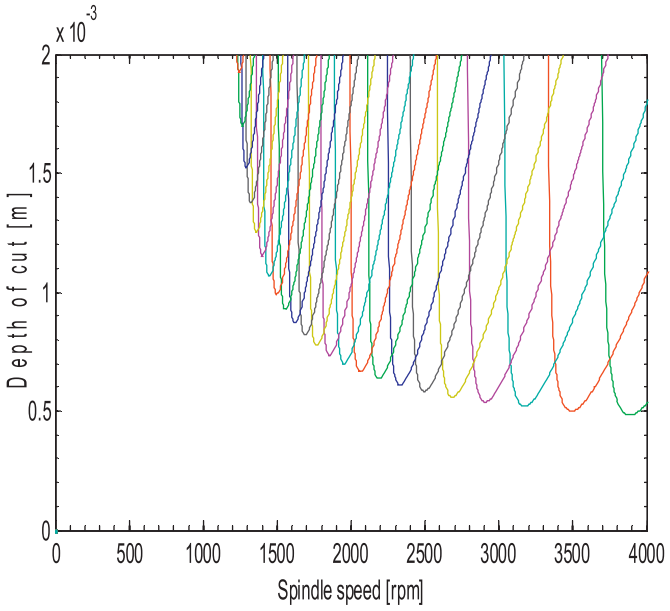

Fig. 5. A twenty iterative computation of stability lobes (l=1 to 60) of the turning process as modelled in this work using the Tyler and Schmitz [20] process damping model.

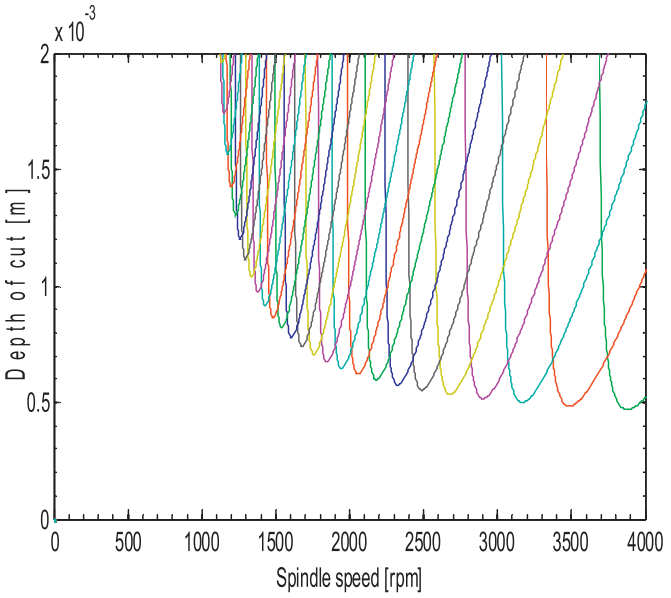

Fig. 7. A twenty iterative computation of stability lobes (l=1 to 60) of the turning process modelled with the proposed process damping model for $\alpha = 0.01$.

$$\Omega_c = 30\omega \left\{ l\pi - \tan^{-1}\left(\frac{\omega_n^2 - \omega^2}{-\left[2\xi\omega_n + \frac{60^{1+\alpha}}{\pi} C_{pd} \frac{w_{c,n-1}}{\Omega_{c,n-1}{}^{1+\alpha} Dm} \nu^{\alpha}\right]\omega} \right) \right\}^{-1} \approx \Omega_{c,n-1},$$
$$l = 1,\ 2,\ 3,\ \ldots \tag{31}$$

The critical depth of cut w_c will subsequently be plotted as a function of critical spindle speed Ω_c to generate the stability lobes of systems with currently proposed process damping model. The numerical parameters of Tyler and Schmitz [20] will be utilized in the next subsection to plot the stability of the turning process on the basis of Eqs. (9), (10), (11), (12), (13), and (14). Thereafter same numerical parameters will be utilized instability analysis of turning with process damping as currently proposed. An effort will be dedicated to determining the approximate value of α that will guarantee the reliability of the proposed model.

3. Results and discussion

3.1. Numerical simulation of stability lobes with process damping

The numerical parameters previously used for simulation are those of a turning process that does not include process damping and thus will not be appropriate for numerical simulation here. Therefore, parameters for numerical simulation are those of the work of Tyler and Schmitz [20]. These parameters which include process damping parameter C_{pd} are listed as follows; natural frequency $\omega_n = 3398.6$ rads^{-1}, damping ratio $\xi = 0.038025$, modal mass $m = 0.561$kg, cutting coefficient $C =$

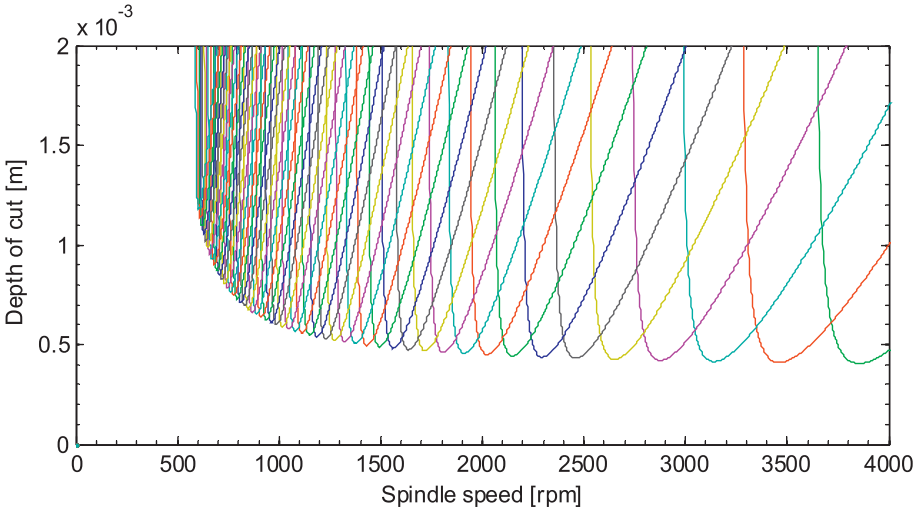

Fig. 6. A twenty iterative computation of stability lobes (l=1 to 60) of the turning process modelled with the proposed process damping model for $\alpha = 0.1$.

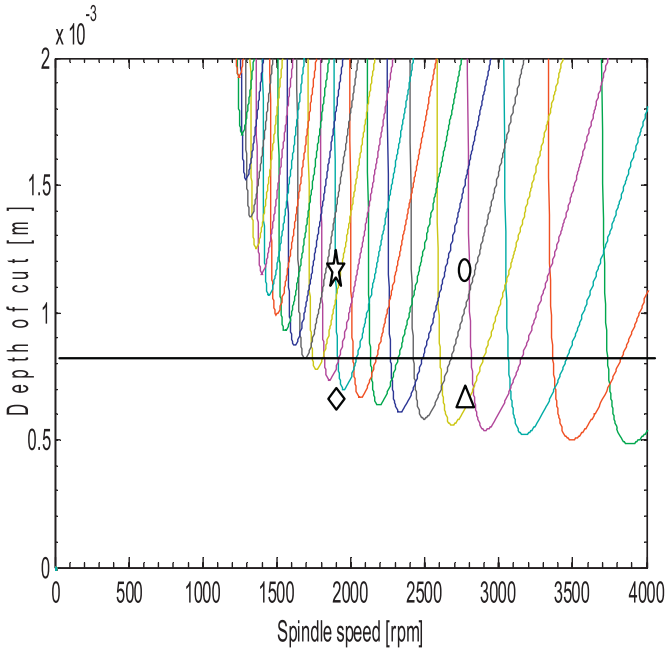

Fig. 8. The four cutting parameter points with process damping chosen for validating time domain simulations.

$1.3755 \times 10^{9}\mathrm{Nm}^{-2}$, feed speed $v = 0.0025\mathrm{ms}^{-1}$, $C_{pd} = 611000\mathrm{Nm}^{-1}$ and $d = 0.035m$. The experimental knowledge that process damping has its maximum stabilizing effect at the lowest speed range is demonstrated in the simulations given as Fig. 2. It is seen in section 2 that within

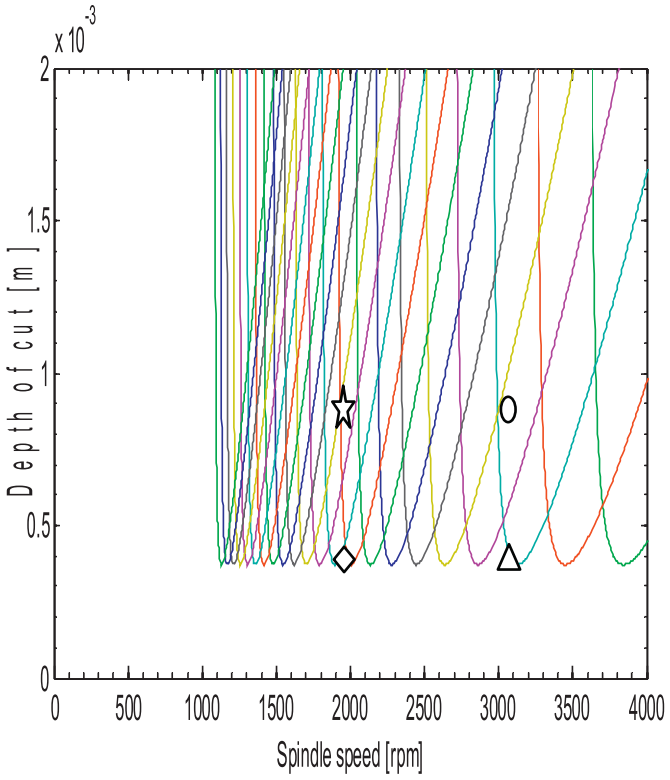

Fig. 9. The four cutting parameter points without process damping chosen for validating time domain simulations.

technological range, the first lobe ($l = 1$) lies in the highest speed range. Generally, an increase in l causes subsequent lobes to shift towards lower speed range. Fig. 2 is generated from Eqs. (11), (12), (13), (14), (15), and (16), which are the equations that are based on Tyler and Schmitz [20] model of process damping. The number attached to a depth of cut symbol w in the legend is equal to the number of iterations leading to the curve. It is seen from Fig. 2a that ten iterations at high-speed range (first lobe) produced coincident lobes. After the first iteration, the subsequent ones generate coincident lobes for the fifth lobe as seen in Fig. 2b. It is seen from Fig. 2c that at a relatively lower speed range of the tenth lobe, ten iterations visibly converged after the second iteration. Iteration converged after first three for the fifteenth lobe as seen in Fig. 2d. Finally, it is seen from Fig. 2e that further lowering of speed range to the twentieth lobe, about five iterations were needed for visible convergence. It must be noted from Fig. 2 that process damping causes stability lobes to shift upwards (stabilizing effect) and slightly to the direction of increasing spindle speed.

The numerical simulation of the proposed process damping model is carried out next. Ten iterations of the proposed process damping model for the case where $\alpha = 0.01$ is carried out leading to the generation of the tenth lobe and twentieth lobe as seen in Fig. 3. It is seen that at low α, iterative convergence of proposed process damping model behaves like the model of Tyler and Schmitz [20]. By increasing α to 0.1 it is seen in Fig. 4 that increase in α hastens the iterative convergence meaning that increase in α cancels process damping effect. This is because every iteration is the same for turning without process damping.fx1

The fact that less number of iterations is needed in Fig. 2 for convergence at higher speed range means that process damping has its maximum stabilizing effect at the lowest speed range. It is seen in Fig. 3 that at low α, iterative convergence of proposed process damping model behaves more or less like the model of Tyler and Schmitz [20]. It is also seen in Fig. 4 that increase in α hastens the iterative convergence meaning that increase in α cancels process damping effect.

The stability diagram of the turning process considering the process damping model of Tyler and Schmitz [20] is shown in Fig. 5. Fig. 5 is a twenty iterative computation of stability lobes of $l = 1$ to 60. Computational validity is guaranteed by comparison with the stability diagram of the same parameters in the work of Tyler and Schmitz [20]. The agreement is seen between the two results in all respects. The validity of this guarantees the analysis of this work in terms of three cardinal aspects which are; formulation of turning process, stability analysis of the turning model on the Laplace variable domain and the iteration schemes presented. These are the three aspects this work physically differs from the most closely related work Tyler and Schmitz [20].

It is seen that the stabilizing effect of process damping disappears with the rise in α in Fig. 6. Process damping is seen to cause a rise in chatter stability at very low spindle speed in Fig. 4. It is seen in Fig. 7 that proposed process damping model behaves more or less like the model of Tyler and Schmitz [20] at low values of α.

3.2. Time-domain simulation of turning process with and without process damping

The capability of MATLAB to simulate time response of systems governed by delay differential equations as provided by the dde23 solver is utilized in this section to further validate the results of this work. The MATLAB dde23 solves delay differential equations with constant delays. The turning models (with and without process damping) considered in this work fall into this category. The basic syntax is; sol = dde23 (*ddefun, lags, history, tspan*) where *ddefun* is the function handle that evaluates the right side of the state space form of the delay differential equation. The *lags* represent a vector of constant positive delays. In the current case, the *lags* is a scalar of value τ. The *history* represents the history of the differential equation. It has been reported in Ozoegwu [19] that the simulation of turning or milling model at given parameter combination gives

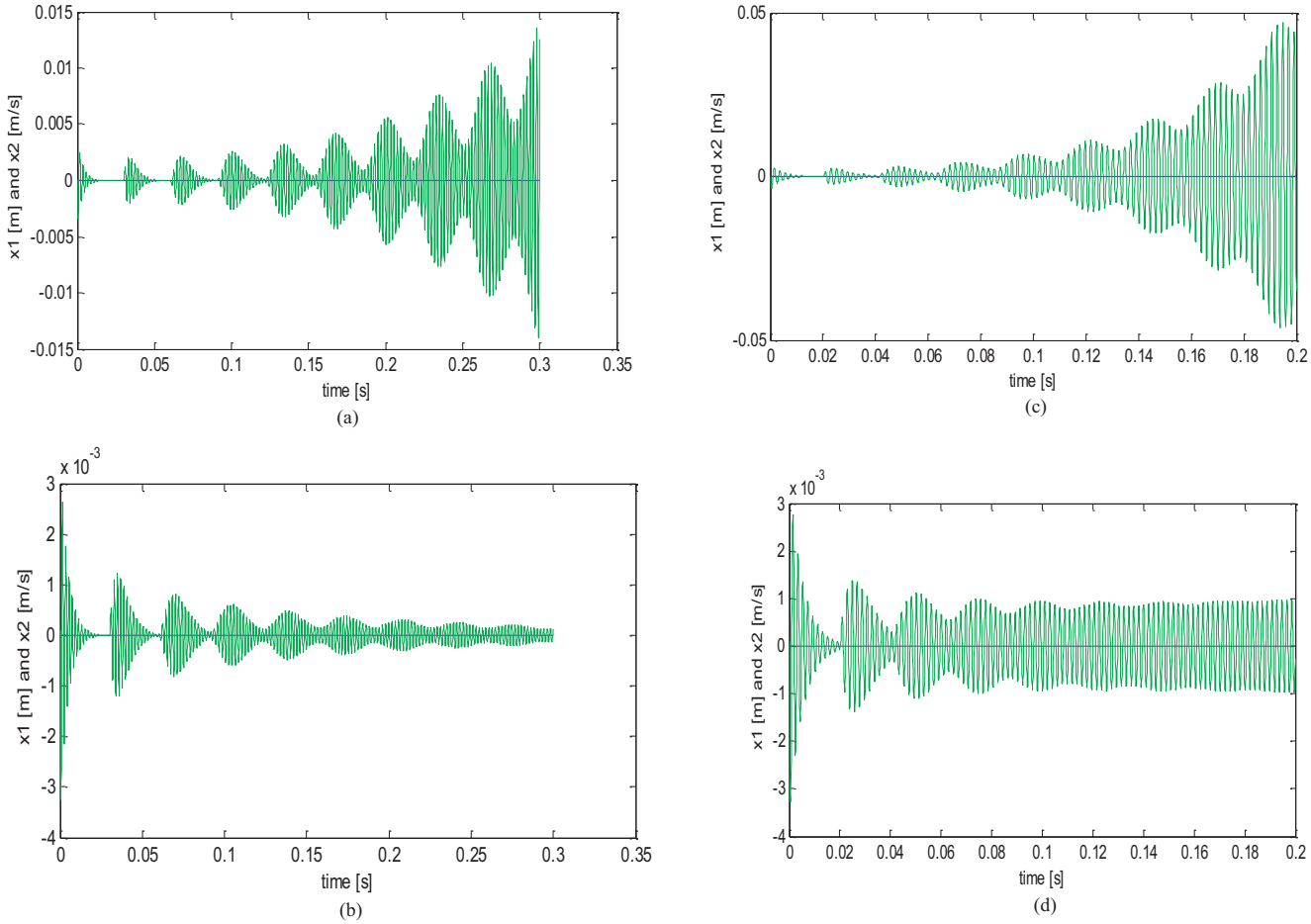

Fig. 10. Time domain simulation of cutting parameter point a) [2000, 0.001] with process damping located as a star on Fig. 8, b) [2000, 0.0005] with process damping located as a diamond on Fig. 8, c) [3000, 0.001] with process damping located as a circle on Fig. 8, d) [3000, 0.0005] with process damping located as a triangle on Fig. 8.

the same result of stability/instability irrespective of the size of the initial condition.

The *tspan* represents the integration interval.

The state space form of Eq. (23) is generated with the substitutions $x_1 = x$ and $x_2 = \dot{x}$ giving;

$$\begin{Bmatrix} \dot{x}_1(t) \\ \dot{x}_2(t) \end{Bmatrix} = \begin{bmatrix} 0 & 1 \\ -\omega_n^2\left(1 - \frac{Cw}{k}\right) & -\left(2\xi\omega_n + \frac{60}{\pi}C_{pd}\frac{w}{\Omega Dm}\right) \end{bmatrix} \begin{Bmatrix} x_1(t) \\ x_2(t) \end{Bmatrix} + \begin{bmatrix} 0 & 0 \\ -\omega_n^2\frac{Cw}{k} & 0 \end{bmatrix} \begin{Bmatrix} x_1(t-\tau) \\ x_2(t-\tau) \end{Bmatrix} \tag{32}$$

The MatLab was used for the simulation of Eq. (31). In order to draw conclusions that validate the stability diagram in Fig. 5 and also validate the known result that process damping stabilizes turning process at low speed, four strategic cutting parameter combinations are considered as shown Figs. 8 and 9. Fig. 8 is same as Fig. 5 with four cutting parameter points [Ω rpm, w m] located namely [2000, 0.001] (star) [2000, 0.0005] (diamond) [3000, 0.001] (circle) and [3000, 0.0005] (circle). The same points are located on an equivalent stability diagram without process damping as shown in Fig. 9. The time domain simulations of the points on Fig. 8 are shown in Fig. 10 while the time domain simulations of the same points on Fig. 9 are shown in Fig. 11. It is seen from Fig. 10 that the time domain simulations agree with the stability diagram as given in either Fig. 5 or Fig. 8. This result clearly attests to the computational accuracy of twenty iterations used in computation either Fig. 5 or Fig. 8. It is also seen from Fig. 11 that the time domain simulations agree with the stability diagram of the equivalent turning process without process damping as given in Fig. 9. Time domain simulations agree with the fact that process damping stabilizes turning process because the stable points in Fig. 8 (diamond and triangle) became unstable points in Fig. 9.

Eq. (32) is used in time domain stimulation in MatLab to get Fig. 10(a – d) at different cutting depths and speed. However, Fig. 11(a – d) were generated by equating $C_{pd} = 0$, hence making all the response to be unstable. The responses being generated are the displacement and velocity of the cutting tool. However the displacement is so small, only velocity responses were visible in the graphs.

In Fig. 8 the points are [2000, 0.001] (star) which is unstable [2000, 0.0005] (diamond) which is stable [3000, 0.001] (circle) which is unstable and (d) [3000, 0.0005] (triangle) which is stable. In Fig. 9, the points are [2000, 0.001] (star) which is unstable [2000, 0.0005] (diamond) which is unstable [3000, 0.001] (circle) which is unstable and (d) [3000, 0.0005] (triangle) which is unstable.

In Fig. 10a the displacement and velocity of the tool increase with time making system to be unstable. Here the displacement and velocity of

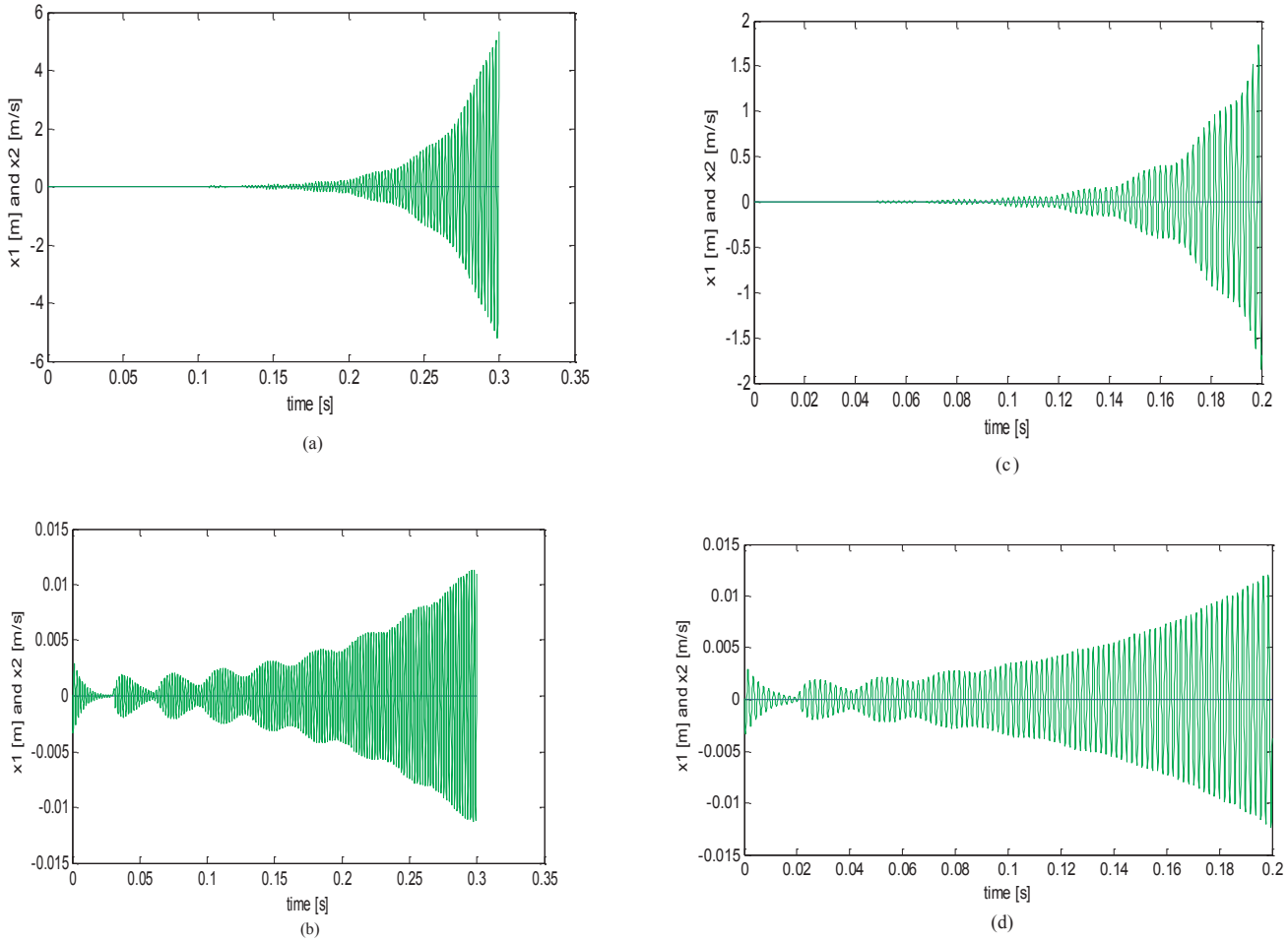

Fig. 11. Time domain simulations of cutting parameter point a) [2000, 0.001] without process damping located as a star on Fig. 9, b) [2000, 0.0005] without process damping located as a diamond on Fig. 9, c) [3000, 0.0005] without process damping located as a triangle on Fig. 9, d) [3000, 0.001] without process damping located as a circle on Fig. 9.

tool grow with time making the system unstable. In Fig. 10b the displacement velocities of tool decay with time making the system to be stable. It is seen in Fig. 10d that the time domain simulations agree with the stability diagram as given in Figs. 5 and 8. Here the displacement and velocity and velocity of the tool stabilize with an increase in time. In Fig. 11, the displacement velocity of the tool increases with time which indicates that the operation is chaotic and unstable. Here, the displacement and velocity of tool grow with time making the system unstable; the displacement and velocity of the tool increase with the increase in time, making the system to be unstable. Time domain simulations agree with the fact that process damping stabilizes turning process.

Table 1
Sound measurements during experimental cutting test.

SN	w = depth of cut (mm)	$\Omega = 200rpm$	$\Omega = 1000rpm$	$\Omega = 4000rpm$
1	0.0	71 dB	74 dB	76 dB
2	0.5	74 dB	78 dB	80 dB
3	1.0	78 dB	84.5 dB	83 dB
4	1.5	79 dB	84.7 dB	104 dB
5	2.0	81.7 dB	108 dB	108 dB
6	2.5	82 dB	110 dB	112 dB
7	3.0	85 dB	112 dB	117 dB
8	3.5	107 dB	115 dB	122 dB

3.3. Experimental validation of the effect of process damping in turning

The observations made in section 2 were summarized in Table 1.

Table 1 was generated during the experimental cutting test to determine the boundary of cut between the stable and unstable cutting process. The decibel value of 85 and below were found to give smooth and stable sounds while the ones above give noisy and rough sounds to the human ear.

It is also seen in Table 1 that stability and smoothness were retained up to a 3mm depth of cut when the spindle speed is low at 200 rpm. For the case where spindle speed is higher at 1000 rpm, stability and smoothness were retained up to a 1.5mm depth of cut. Finally, when the spindle is at its highest speed of 4000 rpm, the system became most unstable. It is then seen from Table 1 that 1mm depth of cut is the threshold for stability for all the cutting speeds. This result is further illustrated in Fig. 12 in which the experimental results are mapped on the plane of spindle speed and depth of cut and an approximate stability curve fixed to demarcate the region of stable and unstable cutting tests. The effect of process damping is obvious as it is seen in Fig. 12 that approximate stability curve gets more stable with a drop in spindle speed.

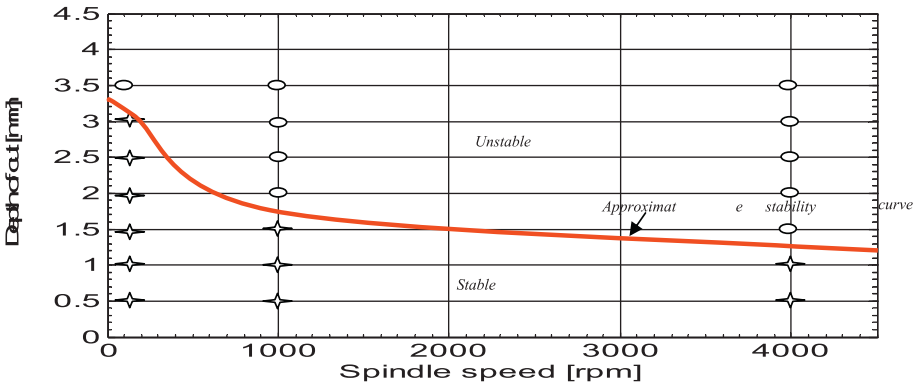

Fig. 12. A graphical representation of cutting tests results showing the approximate stability curve.

Table 2
Theoretical and Experimental Boundary depths.

b_b^{exp}	$b_b^{th}C_{pd}$ = 55000	$b_b^{th}C_{pd}$ = 59000	$b_b^{th}C_{pd}$ = 61000	$b_b^{th}C_{pd}$ = 63000	$b_b^{th}C_{pd}$ = 66000
1.6	1.41	1.55	1.68	1.73	2
1.3	1.18	1.3	1.3	1.4	1.5
1.0	0.98	1.04	1	1.1	1.11
0.9	0.88	0.9	0.915	0.95	0.98
0.8	0.81	0.845	0.86	0.86	0.87

3.4. Estimation of process damping coefficients from cutting tests

Cutting tests were implemented at different spindle speeds and different depths of cut with a blunt tool to maximize process damping effect. At each spindle speed, depth of cut is varied until chatter is noticed. The depth of cut that is midway between the first unstable and last stable depths is noted as the experimental boundary depth b_b^{exp}. Stability curves were generated at different values of process damping coefficients to give theoretical boundary depths b_b^{th} as shown in Table 2.

4. Conclusion

Process damping which was studied happens to be desirable because of its stabilizing effect on low-speed turning process. The process damping model of Tyler and Schmitz [20] was successfully incorporated in the turning stability equations in Ozoegwu [10]. The stability equations were derived using the Laplace transformation method and they differ from those of Tyler and Schmitz [20] which were derived from another line of reasoning based on the frequency response. Exploration for a possible avenue for modification of process damping model of Tyler and Schmitz [20] led to the introduction of non-linear feed term in the process damping model leading to the proposal of process damping force as $F_{pd}(v\tau)^{\alpha}$. It was seen from simulation studies that proposed process damping model behaves more or less like the model of Tyler and Schmitz [20] when α is low. The illustrative low value of α used was 0.01. It was seen that by increasing α to 0.1, the process damping effect is weakened. It was concluded that the proposed process damping model of form $F_{pd}(v\tau)^{\alpha}$ can only be valid for low values of α.

The results of computational processes of turning with process damping were validated by comparison with the computational results in Tyler and Schmitz [20]. Further validation came from simulation using MatLab delay differential equation solver called *dde23,* to simulate vibration response of turning processes at selected points on the stability diagram of turning with and without process damping. Simulations in (for example those in Fig. 10 were seen to agree with the stability diagrams (for example that in Fig. 9 attesting to the computational accuracy of twenty iterations used in the computation of stability diagram with process damping. Additionally, simulation results reinforced the fact that process damping stabilizes turning process because the stable points in stability diagram of turning with process damping became unstable points in the stability diagram of turning without process damping. Finally, three different spindle speed range of 200 *rpm*, 1000 *rpm*, and 4000 *rpm* were chosen and their respective experimental depths of cut measured. These experimental depths of cut were superimposed on different stability diagrams with known coefficient of process damping.

Declarations

Author contribution statement

Jeremiah Chukwuneke: Analyzed and interpreted the data; Wrote the paper.

Sam Omenyi: Conceived and designed the experiments.

Chinedu Izuka: Performed the experiments; Contributed reagents, materials, analysis tools or data.

Funding statement

This research did not receive any specific grant from funding agencies in the public, commercial, or not-for-profit sectors.

Competing interest statement

The authors declare no conflict of interest.

Additional information

No additional information is available for this paper.

References

[1] R. Paurobally, M. Siddhpura, A review of chatter vibration research in turning, Int. J. Mach. Tool Manuf. 61 (2012) 27–47.
[2] E. Turkes, S. Neseli, A simple approach to analyze process damping in chatter vibration, Int. J. Adv. Manuf. Technol. 70 (5-8) (2013) 775–786.
[3] T.G. Molnar, D. Bachrathy, T. Insperger, G. Stepan, On process damping induced by vibration-dependency of cutting direction in milling, Procedia CIRP 1 – 4 (2018).
[4] Y. Altintas, M. Weck, Chatter stability of metal cutting and grinding, CIRP Ann. – Manuf. Technol. 53 (2004) 619–642.
[5] A.M.F. Mubarack, Z. Haitao, A.W. Hassan, Damping effect on chatter stability of turning and milling processes, JVE procedia 13 (2017) 7–14.
[6] L.T. Tunc, E. Budak, Effect of cutting conditions and tool geometry on process damping in machining, Int. J. Mach. Tool Manuf. (2012) 5710–5719.
[7] C.G. Ozoegwu, Stability wave attenuation effects in turning process, Prod. Manuf. Res. 2 (1) (2014) 2–10.
[8] Y. Altintas, E. Budak, Analytical prediction of stability lobes in milling, CIRP Ann. - Manuf. Technol. 44 (1) (1995) 357–362, 1995.
[9] G. Arten, G. Mikhail, A. Gouskov, P. Lorong, A. Shokhin, An analytical modelling of a thin-walled cylindrical workpiece during turning process: stability analysis of a cutting process, Int. J. Mach. Mach. Mater. 19 (1) (2017) 17–40.
[10] T.C. Tyler, L.T. Schmitz, Process damping analytical stability analysis and validation, Proc. NAMRI/SME 40 (2012) 1–11.

[11] Y. Kurata, S.D. Merdol, Y.N. Altintas, N. Suzuki, E. Shamoto, Chatter stability in turning and milling with in process identified process damping, J. Adv. Mech. Des. Sys. Manu. 4 (2010) 1107–1118.
[12] Z.Z.F. Li, A.D. Yafeng, L. Xia, Y. Peng, Modelling and simultation of cutting stability considering process damping, J. Hunan Univ. Tech. 28 (6) (2014) 23–26.
[13] X. Li, W. Zhao, L. Li, N. He, S.W. Chi, Modelling and application of process damping in milling of thin-walled workpiece made of Titanium Alloy, Shock Vib. (2015).
[14] Y. Altintas, Manufacturing Automation, Metal Cutting Mechanics, Machine Tool Vibrations, and CNC Design, Cambridge University Press, USA, 2000, p. 61.
[15] G. Byrne, D. Dornfeld, I. Inasaki, G. Ketteler, W. Konig, R. Teti, Tool condition monitoring (TCM) – the status of research and industrial application, CIRP Ann. – Manuf. Technol. 44 (2) (1995) 541–567.
[16] K. Ahmadi, F. Ismail, Analytical stability lobes including nonlinear process damping effect on machining chatter, Int. J. Mach. Tool Manuf. 51 (2011) 296–308.
[17] E. Budak, L. Tunc, Identification and modelling of process damping in turning and milling using a new approach, CIRP Ann. – Manuf. Technol. 59 (1) (2010) 403–408.
[18] T.G. Molnar, T. Insperger, D. Bachrathy, G. Stepan, Extension of process damping to milling with low radial immersion, Int. J. Adv. Manuf. Technol. 89 (9-12) (2016) 2545–2556.
[19] C.G. Ozoegwu, Chatter of Plastic Milling CNC Machine, M.Eng Thesis, Nnamdi Azikiwe University, Awka, Nigeria, 2011.
[20] T.C. Tyler, L.T. Schmitz, Analytical process damping stability prediction, J. Manuf. Process. 15 (2013) 69–76.
[21] Y. Altintas, M. Eynian, H. Onozuka, Identification of dynamic cutting force coefficients and chatter stability with process damping, CIRP Ann. - Manuf. Technol. 57 (2008) 371–374.
[22] M.K. Dikshit, A.B. Puri, A. Maity, Chatter and dynamic cutting force prediction in high-speed ball end milling, J. Mach. Sci. Tech. 21 (2) (2017) 291–312.
[23] C.G. Ozoegwu, S.N. Omenyi, Stability characterization of a turning process, J. Eng. Appl. Sci. 8 (1) (2012) 68–75.
[24] J.L. Chukwuneke, C.H. Achebe, S.N. Omenyi, C.G. Ozoegwu, Chatter stability characterization of plastic end – milling CNC machine, Innov. Syst. Des. Eng. 3 (11) (2012) 17–28.
[25] O. Gurdal, E. Ozturk, N.D. Sims, Analysis of process damping in milling, Procedia CIRP 55 (2016) 152–157.